Materials Research Bulletin 145 (2022) 111535

Contents lists available at ScienceDirect

Materials Research Bulletin

journal homepage: www.elsevier.com/locate/matresbu

Research Papers

Intense and efficient green mechanoluminescence in $CaLaAl_3O_7$ through Tb^{3+} doping

Shiye Qin [a,b], Jiali Bian [a,b], Yue Han [b,c], Zhidong Ma [b], Bin Liu [c], Jiachi Zhang [a,*], Xuhui Xu [d], Zhaofeng Wang [b,*]

[a] National & Local Joint Engineering Laboratory for Optical Conversion Materials and Technology, Lanzhou University, Lanzhou, Gansu 730000, China
[b] State Key Laboratory of Solid Lubrication, Lanzhou Institute of Chemical Physics, Chinese Academy of Sciences, Lanzhou, Gansu 730000, China
[c] School of Stomatology, Lanzhou University, Lanzhou, Gansu, 730000, China
[d] College of Materials Science and Engineering, Kunming University of Science and Technology, Kunming, Yunnan 650093, China

ARTICLE INFO

Keywords:
A. Inorganic compounds
b. Luminescence
d. Phosphors

ABSTRACT

In this work, an efficient mechanoluminescent material with green emitting color, $CaLaAl_3O_7:Tb^{3+}$, is reported. The mechanoluminescent intensity of $CaLaAl_3O_7:Tb^{3+}$ is dependent on the content of luminescent centers, and the optimum doping concentration of Tb^{3+} is determined to be 6.0%, whatever the sample is stimulated by stretching or rubbing. The temperature-dependent properties suggest that the mechanoluminescence of $CaLaAl_3O_7:Tb^{3+}$ should come from the released carriers from traps under stress stimuli, and therefore the underlying mechanoluminescent mechanisms of $CaLaAl_3O_7:Tb^{3+}$ is revealed. By comparing with the commercial ZnS:Cu, a well-known mechanoluminescent material with high efficiency, the $CaLaAl_3O_7:Tb^{3+}$ exhibits an even higher intensity when tested at the same conditions. It suggests that $CaLaAl_3O_7:Tb^{3+}$ is a very efficient mechanoluminescent material, showing promising applications in the new generation of lighting, displaying and sensing devices.

1. Introduction

Mechanoluminescence (ML) is a light-emitting phenomenon when a material is stimulated by various mechanics, such as compressing, stretching, bending, rubbing, impact, *etc.* [1-4]. Compared with the other types of luminescence, ML has great advantages in energy saving and convenience, and therefore it shows wide application prospects in the fields of lighting, displaying, and visualized sensing [5-10]. In the above applications, ML material with green emission color plays a key role, because green is one of the most easily captured colors for human eyes. At present, three kinds of systems, *i.e.*, ZnS:Cu, $CaZnOS:Tb^{3+}$ and $SrAl_2O_4:Eu^{2+},Dy^{3+}$, are well-accepted as the green ML materials with high performance [11-13]. However, ZnS:Cu and $CaZnOS:Tb^{3+}$ contain the sulfur source, resulting in the environmental pollution during synthesis. For the system of $SrAl_2O_4:Eu^{2+},Dy^{3+}$, the prominent long afterglow behavior causes inevitable interference on the measurement and analysis of ML signal [14,15]. Herein, it is necessary to develop novel ML materials with green emitting color towards environmental protection, high ML efficiency and free from afterglow interference.

The selection of matrix and doped ion is extremely important in the design of luminescent materials. Aluminate $ABAl_3O_7$ with melilite structure (A is Ca, Sr or Ba, and B is La, Gd or Y) is an important matrix for luminescence, which belongs to $P42_1m$ space group with a layered structure formed by $[AlO_4]^{5-}$ tetrahedra [16,17]. Structural analysis shows that A^{2+} and B^{3+} are both eight coordinated occupying the same 4e sites, and hence there are abundant defects/traps in the $ABAl_3O_7$ matrix itself, which could be further regulated by rare earth ion doping [18]. This provides great feasibility for the generation of ML [19]. For the doped ions, Tb^{3+} is a well-known activation ion with green emitting color, which is produced by the typical $^5D_4 \rightarrow {}^7F_J$ (J=3,4,5,6) transitions. The dopant of Tb^{3+} has the advantages of large absorption coefficient, high luminescence intensity and stable luminescence [20,21]. Therefore, it is feasible to achieve green ML by doping Tb^{3+} ions in the melilite structure.

Inspired by the above considerations, in this work, we doped Tb^{3+} in a typical melilite structure, $CaLaAl_3O_7$, and investigated its ML properties. The results suggest that $CaLaAl_3O_7:Tb^{3+}$ exhibits extremely intense green ML, which is even higher than that of the commercial ZnS:

* Corresponding authors.
E-mail addresses: zhangjch@lzu.edu.cn (J. Zhang), zhfwang@licp.cas.cn (Z. Wang).

https://doi.org/10.1016/j.materresbull.2021.111535
Received 15 July 2021; Received in revised form 10 August 2021; Accepted 23 August 2021
Available online 28 August 2021

Cu. By understanding the stimulation/activation and radiative transfer processes, the underlying mechanisms of $CaLaAl_3O_7:Tb^{3+}$ is revealed.

2. Experimental

2.1. Synthesis of $CaLaAl_3O_7:Tb^{3+}$ powders

A series of $CaLaAl_3O_7:xTb^{3+}$ (x=4.0%, 5.0%, 6.0%, 7.0%, 8.0%) powders were synthesized by a high-temperature solid-state method. The raw materials of $CaCO_3$ (99.99%), La_2O_3 (99.99%), Al_2O_3 (99.70%), and Tb_4O_7 (99.99%) were accurately weighed by stoichiometric ratios and put into an agate mortar. Then, the mixture was dispersed in a certain amount of alcohol and fully ground. After that, the mixture was transferred into a corundum crucible and placed in a muffle furnace. The mixture was kept at 1600 ℃ for 5 h in a reducing atmosphere composed of nitrogen and hydrogen (90%N_2 and 10%H_2 in volume ratio). After cooling to room temperature, the sample was taken out and $CaLaAl_3O_7:Tb^{3+}$ was finally obtained.

2.2. Preparation of $CaLaAl_3O_7:Tb^{3+}$/PDMS composites

Polydimethylsiloxane (PDMS) was chosen as the flexible matrix for $CaLaAl_3O_7:Tb^{3+}$ powders to facilitate the ML measurement and analysis. First, 2.0 g of PDMS precursor and 0.2 g of curing agent were placed in a dumbbell-shaped mode with a effective length of 25 mm and a width of 10 mm. Then, 1.0 g of the $CaLaAl_3O_7:Tb^{3+}$ powders were mixed. After mechanical stirring for 30 min, the mixture was put into a vacuum oven at room temperature and -8.6×10^4 Pa for 15 min. Finally, the sample was cured at 70 ℃ for 1 h in a regular oven, and the $CaLaAl_3O_7:Tb^{3+}$/PDMS composite elastomer was obtained.

2.3. Characterizations

X-ray diffractometer (XRD) of Auriga Shimadzu/XRD-6100 was used to analyze the crystalline structure of the phosphor. The working voltage is maintained at 220 V, and the excitation source is Cu Kα (1.54056 Å) with a scanning step of 0.02° and a scanning speed of 10°/min in a scanning range of 10° - 80°. The micro-morphology and elemental distribution of $CaLaAl_3O_7:Tb^{3+}$ powders were characterized by a field emission scanning electron microscopy (FE-SEM, JSM-6701F, Hitachi) and scanning electron microscopy (EDS, JSM-5601LV, Hitachi), respectively. Photoluminescence (PL) and photoluminescence excitation (PLE) spectra were recorded using a fluorescence spectrometer (Omni-300i) with Xe900 lamp (500 W) as excitation source. The thermoluminescence (TL) curve was detected by a FJ-427A TL measuring instrument. The stretching experiments of $CaLaAl_3O_7:Tb^{3+}$/PDMS elastomer were conducted on a self-made tensile testing machine, with the effective sample size of 25×10×2 mm, the stretching frequency of 3 Hz and the maximum stretching strain of 80%. The rubbing experiments were operated on a rotary friction testing machine (MS-T3001) using the stainless-steel rod (radius: 0.2 mm) as the friction pair. The applied load and rotational speed were set to 4.9 N and 200 r/min, respectively. The produced ML signals during mechanics stimuli were collected through a spectrometer (Omni-λ300i, Zolix Instruments Co, Ltd) equipped with a CCD camera (IVAC-316, Edmund Optics Ltd.).

3. Results and discussion

Fig. 1a shows the XRD patterns of the $CaLaAl_3O_7:xTb^{3+}$ (x=4.0%, 5.0%, 6.0%, 7.0%, 8.0%) samples synthesized by the solid-state method. It is observed that all diffraction peaks match well with the standard JCPDS card (No.81-1719), indicating that the as-synthesized samples are of single phase and the doping of Tb^{3+} in $CaLaAl_3O_7$ could not arouse any impurity peaks. It is also found in Fig. 1a that with the increase of the doping concentration of Tb^{3+}, the (211) peak at 30.904° exhibits a slight shift to high position. According to the Bragg's law $2d\sin\theta = n\lambda$, where d is the spacing of the parallel atomic plane, λ is the wavelength of the incident wave, and θ is the angle between the incident light and the crystal plane, the increased θ value of (211) peak corresponds to the decrease of d spacing with the increase of the Tb^{3+} content. Hence, it suggests that Tb^{3+} should substitute the cations in $CaLaAl_3O_7$ with a larger ionic radius. By comparing the ionic radius of Ca^{2+} (CN=8, $R_{Ca}{}^{2+}$=0.112 nm), La^{3+} (CN=8, $R_{La}{}^{3+}$=0.116 nm) and Al^{3+} (CN=4, $R_{Al}{}^{3+}$=0.039 nm) and Tb^{3+} (CN=8, $R_{Tb}{}^{3+}$=0.104 nm), and combining the Hume-Rothery principle, it is determined that Tb^{3+} should occupy the lattice position of La^{3+} [22,23]. Fig. 1b presents the crystal structure of $CaLaAl_3O_7$, which has a layered melilite structure with a space group of $P42_1m$. The layer of the compound is composed of $[AlO_4]^{5-}$ tetrahedra formed by Al and O through four coordination. The interlayer is composed of Ca^{2+} and La^{3+} cations with octahedral Cs symmetry by alternating distribution. The alternating layer is conducive to the direct excitation of rare earth ions from the ground state energy level to the excited state energy level, which provides the effective pathways for the doped rare earth ions to emit various luminescence [24].

SEM and EDS mappings were further employed to investigate the morphology and chemical composition of the $CaLaAl_3O_7:Tb^{3+}$. As shown in Fig. 2a and b, the as-synthesized $CaLaAl_3O_7:Tb^{3+}$ exhibits a remarkable layered structure which is in good agreement with its crystal characteristics. The EDS mappings in Fig. 2c confirm that the sample is composed of Ca, La, Al, O and Tb. All of the results raised by XRD and

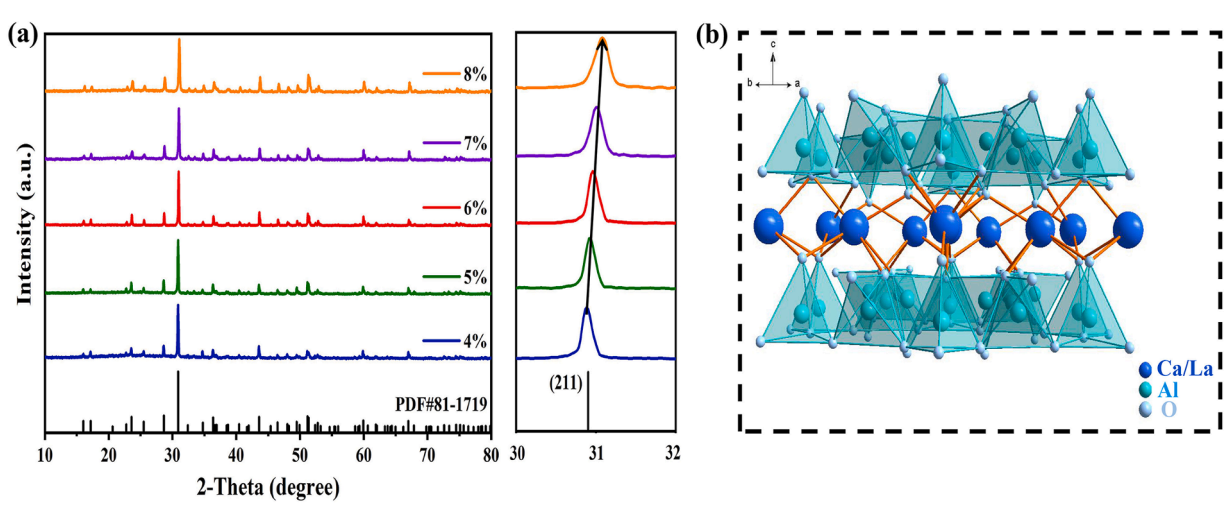

Fig. 1.. (a) XRD patterns of $CaLaAl_3O_7:xTb^{3+}$ (x=4.0%–8.0%) samples; (b) Crystal structure of $CaLaAl_3O_7$.

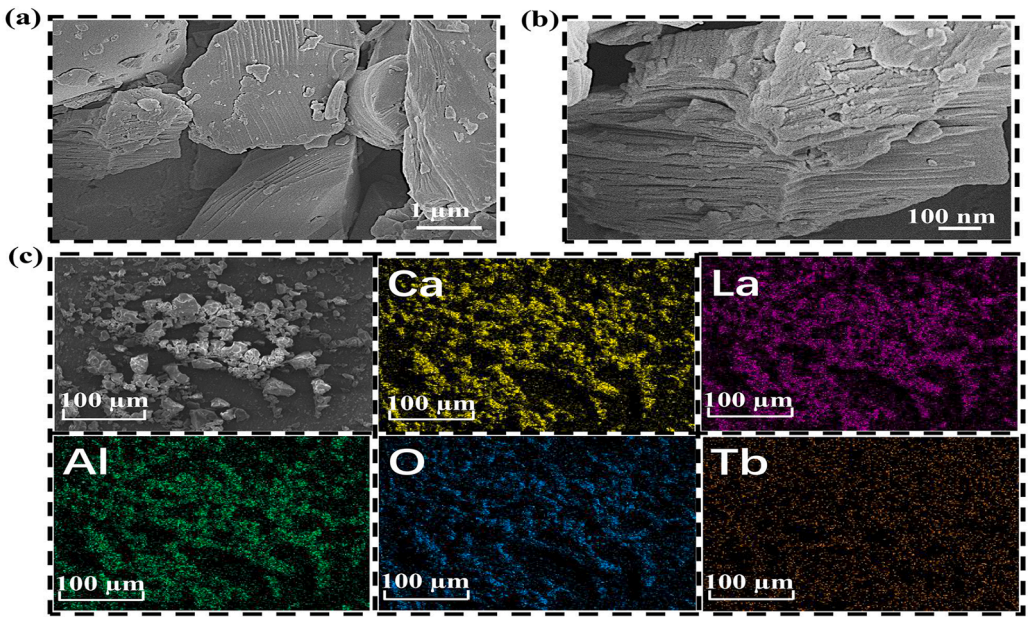

Fig. 2.. SEM images of $CaLaAl_3O_7$:6%Tb^{3+} in a relatively (a) low and (b) high magnification; (c) EDS mappings of the $CaLaAl_3O_7$:6%Tb^{3+} sample.

SEM suggest that single phase $CaLaAl_3O_7$:Tb^{3+} with a layered structure has been successfully obtained.

After doping Tb^{3+} ions, the samples could exhibit intense PL. Fig. 3a shows the excitation spectra of the as-synthesized $CaLaAl_3O_7$:Tb^{3+} monitored at 545 nm. The excitation peaks at 285, 320, 344, 354 and 375 nm should be originated from the characteristic transitions of Tb^{3+} ions in the pathways of $4f^8 \rightarrow 4f^7 5d^1$, $^7F_6 \rightarrow {}^5D_1$, $^7F_6 \rightarrow {}^5G_2$, $^7F_6 \rightarrow {}^5D_2$ and $^7F_6 \rightarrow {}^5L_{10}$, respectively [25,26]. When excited by a 375 nm light, the $CaLaAl_3O_7$:Tb^{3+} exhibits characteristic emissions of Tb^{3+} at 415, 438, 457, 493, 545, 590 and 623 nm (as shown in Fig. 3b), attributed to the transitions of $^5D_3 \rightarrow {}^7F_J$ (J=6, 5, 4) and $^5D_4 \rightarrow {}^7F_J$ (J=6, 5, 4, 3), respectively [27,28]. It is observed in both of the excitation and emission spectra that the luminescent intensity is strongly dependent on the doping concentration of Tb^{3+}, and the optimum Tb^{3+} content is 6.0%. This is because with the increase of Tb^{3+} doping concentration, the luminescent centers increase, and the luminescence intensity increases accordingly. However, when the concentration of Tb^{3+} increases to a certain extent with the distance between luminescence centers less than the critical value, the cross-relaxation between luminescence centers will be dominant, resulting in non-radiative transitions and luminescence quenching [29].

To facilitate the ML investigation, $CaLaAl_3O_7$:Tb^{3+} powders were further composited into PDMS flexible matrix because of its high transparency and efficient stress transfer ability [30]. When stimulated by stretching or rubbing, the $CaLaAl_3O_7$:Tb^{3+} samples embedded in PDMS elastomer exhibit intense green ML, as shown in Fig. 4. The ML spectra of $CaLaAl_3O_7$:Tb^{3+} in Fig. 4a and b are similar with its PL properties that it presents characteristic emissions of Tb^{3+} at 411, 435, 455, 491, 544, 589 and 622 nm, corresponding to the transitions of $^5D_3 \rightarrow {}^7F_J$ (J=6, 5, 4) and $^5D_4 \rightarrow {}^7F_J$ (J=6, 5, 4, 3), respectively [31]. It suggests that the emitting processes of the ML of $CaLaAl_3O_7$:Tb^{3+} should also come from the radiative transfer among the energy levels of Tb^{3+}. Fig. 4c and d show the ML intensity variations of $CaLaAl_3O_7$:Tb^{3+} in PDMS along with the change of the Tb^{3+} concentration under the stimulation of stretching and rubbing. It is obvious that with the increase of the doping concentration of Tb^{3+}, the ML of $CaLaAl_3O_7$:Tb^{3+} increases first and then decreases due to the concentration quenching, and the optimum doping content of Tb^{3+} for the ML is also determined to

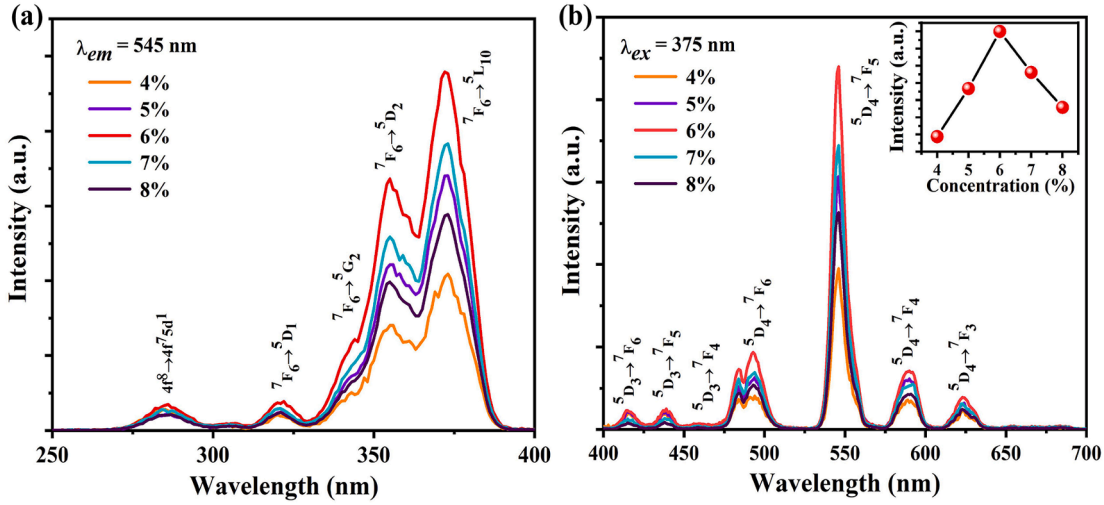

Fig. 3.. (a) Excitation spectra of $CaLaAl_3O_7$:xTb^{3+} (x=4.0%, 5.0%, 6.0%, 7.0%, 8.0%) monitored at 545 nm; (b) Emission spectra of $CaLaAl_3O_7$:xTb^{3+} (x=4.0%, 5.0%, 6.0%, 7.0%, 8.0%) under the excitation of 375 nm; the inset in (b) shows the PL intensity variations with the increase of Tb^{3+} content.

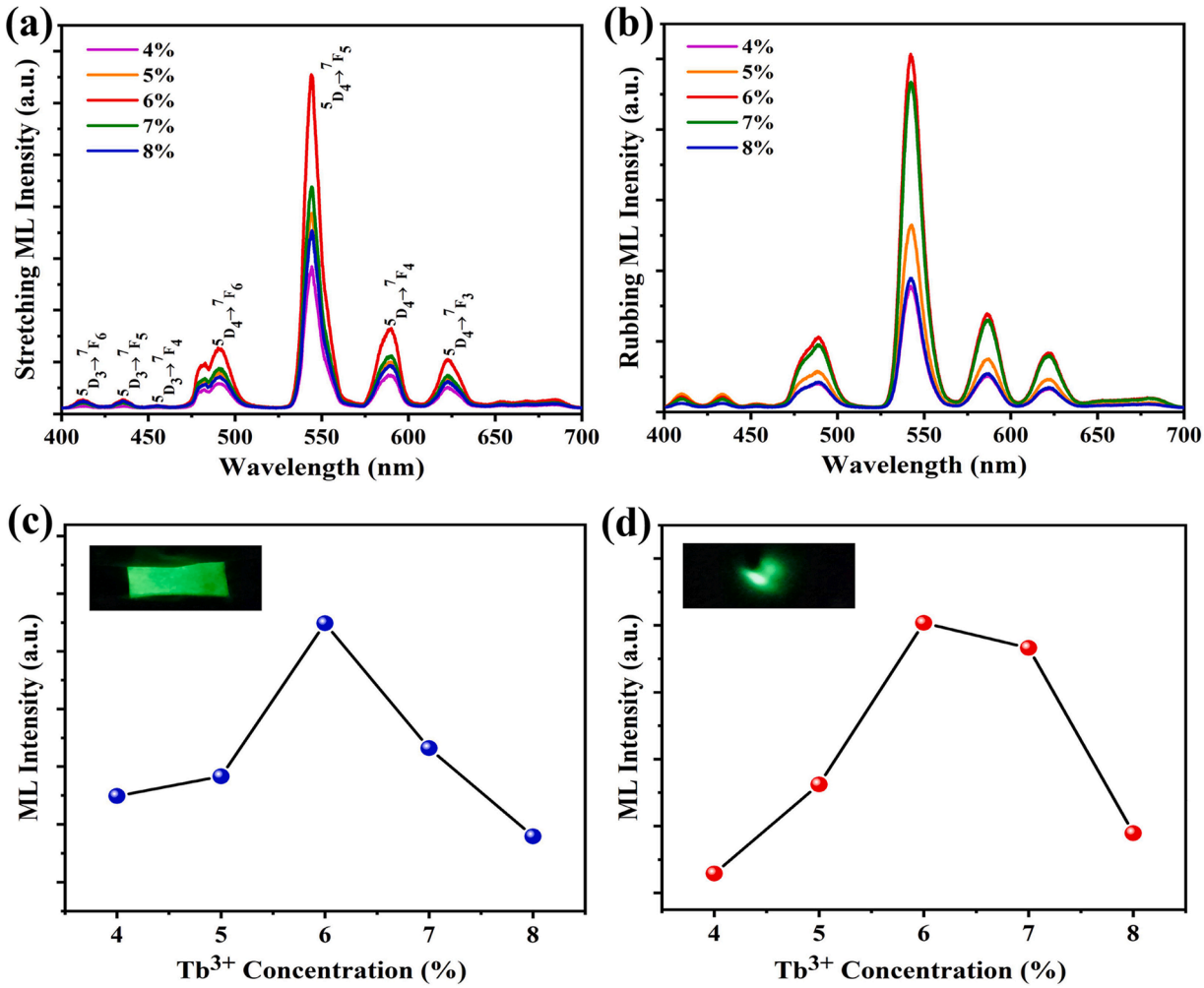

Fig. 4.. ML spectra of $CaLaAl_3O_7$:xTb^{3+}(x=4.0%, 5.0%, 6.0%, 7.0%, 8.0%)/PDMS composites under the stimulation of (a) stretching and (b) rubbing; ML intensity variations of $CaLaAl_3O_7$:Tb^{3+} accompanied by the change of Tb^{3+} concentration under the stimulation of (c) stretching and (d) rubbing; the insets in (c) and (d) present the ML photos of the $CaLaAl_3O_7$:Tb^{3+} in PDMS elastomer under stretching and rubbing, respectively.

6.0%.

In addition to the emission properties, it is necessary to reveal the stimulation/activation processes of the ML of $CaLaAl_3O_7$:Tb^{3+} to understand the underlying ML mechanisms. Fig. 5 shows the TL and ML properties of the $CaLaAl_3O_7$:Tb^{3+} after various heat treatments from 298 to 473 K. It is observed in Fig. 5a that with the increase of the treated temperature, the TL intensity of $CaLaAl_3O_7$:Tb^{3+} is gradually decreased with the spectra narrowed and red-shifted. This is because that the pre-heat treatment could clear the carriers in the shallow trap first and then those in the deep trap [32]. The detailed trap information in $CaLaAl_3O_7$:Tb^{3+} including the trap types and trap depths could be revealed following the Eqs. (1)-(2)[33,34],

$$I(T) = Cexp(-E/KT) \tag{1}$$

$$LnI(T) = -E/KT + LnC \tag{2}$$

where $I(T)$ represents the TL tensity, C is a constant including frequency factor s, K denotes the Boltzmann constant, E is the shallowest trap depth, and T represents temperature. Herein, Fig. 5a is further transformed to the curves of $1000/T$ *vs.* Ln(TL intensity) as shown in Fig. 5b, and the slope of each curve in Fig. 5b represents the value of $-E/K$. Accordingly, the shallowest trap depth E of $CaLaAl_3O_7$:Tb^{3+} after various pre-heat treatment is obtained, as illustrated in Fig. 5c, which contains two linear stages suggesting that there are two types of traps (trap 1 and trap 2) in the structure of $CaLaAl_3O_7$:Tb^{3+} with the trap depth in the range of 0.10-0.66 eV and 0.66-0.70 eV, respectively. In order to investigate the effects of traps on the ML performance, the ML spectra of $CaLaAl_3O_7$:Tb^{3+} after various pre-heat treatments from 298 to 473 K were also measured. As shown in Fig. 5d, the ML intensity of $CaLaAl_3O_7$:Tb^{3+} exhibits a similar decreasing trend to that of the carrier density in traps. It provides a direct evidence that the release of trapped carriers under the mechanical stimuli should be the origination of ML in $CaLaAl_3O_7$:Tb^{3+}.

Based on the PL, ML and TL analysis as well as the temperature-dependent behaviors, the luminescent mechanisms of $CaLaAl_3O_7$:Tb^{3+} are illustrated in Fig. 6. The ① and ② show the PL processes, in which electrons are excited to the $^5L_{10}$ level of Tb^{3+} first and then relaxed to the $^5D_3$ and $^5D_4$ levels to generate luminescence. ③-⑧ illustrate the processes of ML. Under stress stimuli, the electrons in traps could be released to the conduction band (CB) first and then to the $^5F_7$ level of Tb^{3+}. By relaxation to the $^5D_3$ and $^5D_4$ levels, the electrons could recombine the holes in ^7F_J (J=3, 4, 5, 6) levels, producing the as-observed green ML.

To well perceive the ML performance of $CaLaAl_3O_7$:Tb^{3+}, it is further compared to the commercial ZnS:Cu sample which is widely accepted as one of the most efficient ML materials. Fig. 7a shows the comparison of the ML spectra of $CaLaAl_3O_7$:6.0%Tb^{3+} and ZnS:Cu in PDMS elastomer under the same stretching conditions (effective sample size: 25×10×2 mm; powder to elastomer ratio: 1:2; stretching frequency: 3 Hz; maximum stretching strain: 80%). It is found that the maximum ML

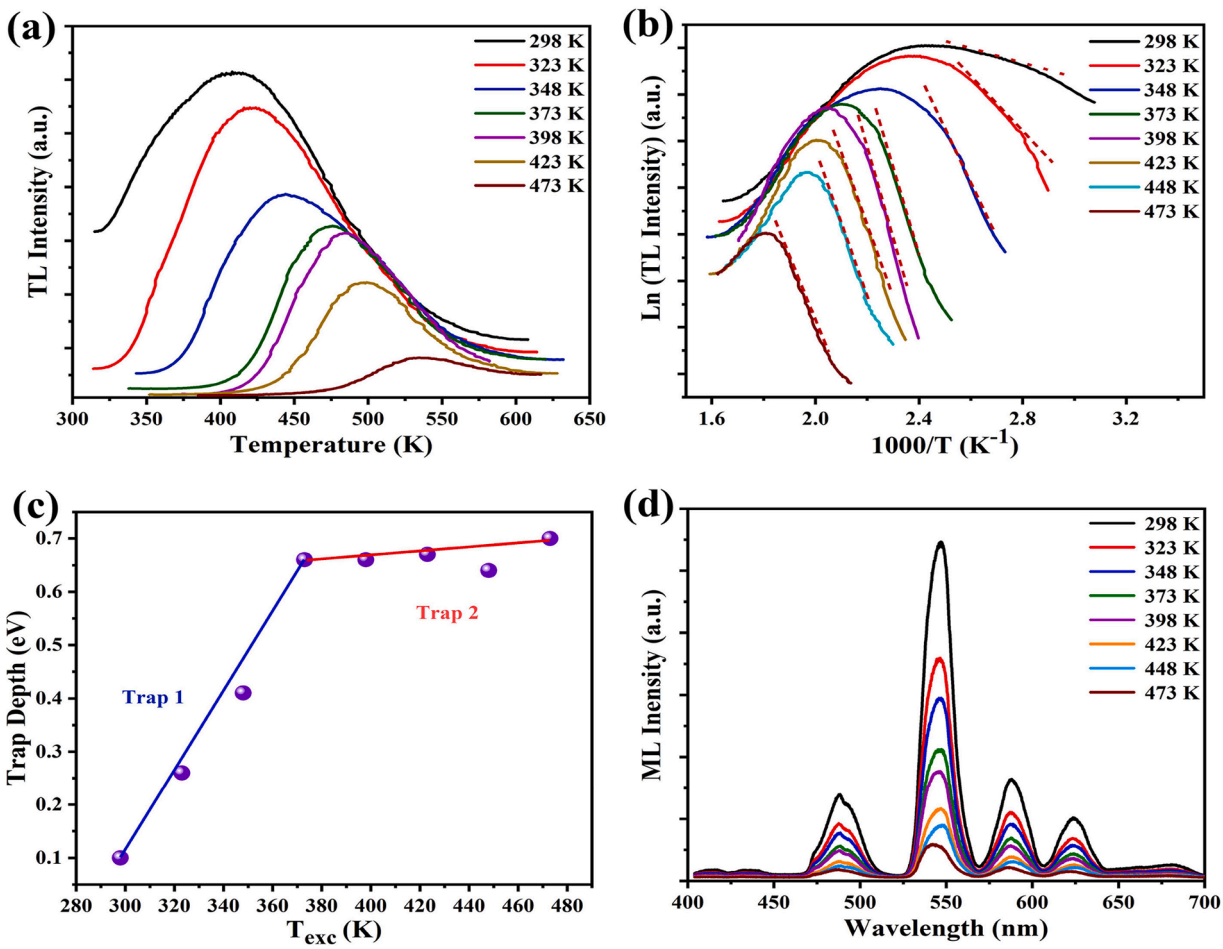

Fig. 5.. (a) TL spectra of $CaLaAl_3O_7$:6%Tb^{3+} after pre-heat treatments from 298 to 473 K; (b) 1000/*T* vs. *Ln*(TL intensity) curves transformed from (a); (c) Trap depth variation in $CaLaAl_3O_7$:6%Tb^{3+} after various pre-heat treatments; (d) ML spectra of $CaLaAl_3O_7$:6%Tb^{3+} after pre-heat treatments from 298 to 473 K.

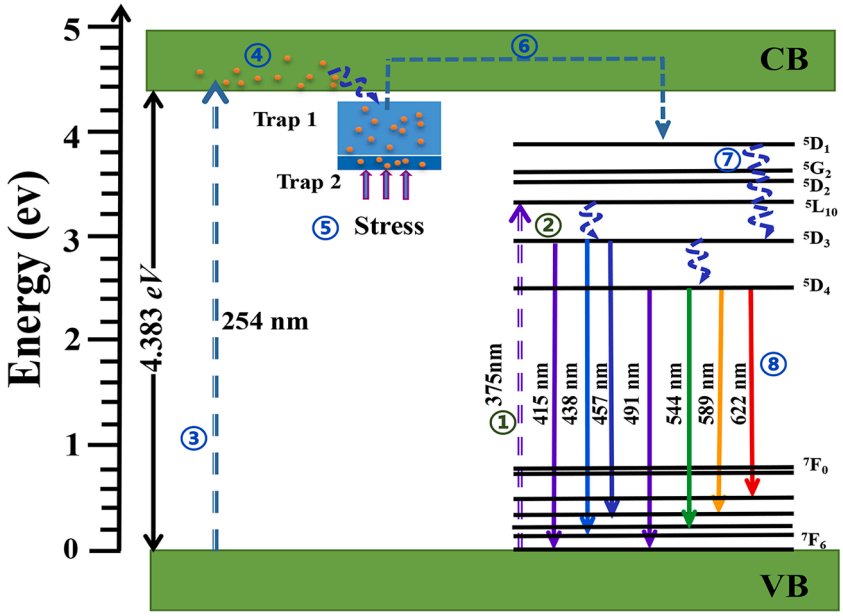

Fig. 6.. PL and ML processes of the $CaLaAl_3O_7$:Tb^{3+} in the energy level diagram.

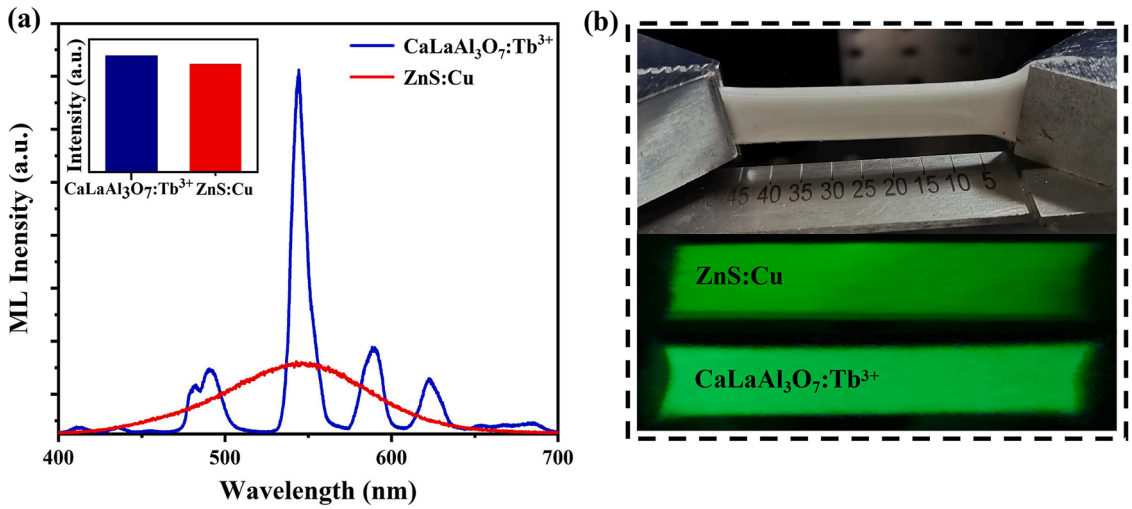

Fig. 7. (a) Horizontal comparison of the ML spectra of $CaLaAl_3O_7$:6.0%Tb^{3+} and ZnS:Cu tested at the same conditions (effective sample size: 25×10×2 mm; powder to elastomer ratio: 1:2; stretching frequency: 3 Hz; maximum stretching strain: 80%); (b) ML photos of $CaLaAl_3O_7$:6.0%Tb^{3+} and ZnS:Cu in PDMS elastomers.

peak of $CaLaAl_3O_7$:Tb^{3+} is higher than that of ZnS:Cu, and the integrated ML intensity of $CaLaAl_3O_7$:6.0%Tb^{3+} reaches 1.3 times of that of the ZnS:Cu. The color coordinates of the ZnS:Cu and $CaLaAl_3O_7$:Tb^{3+}-based elastomers are calculated to be (0.33,0.46) and (0.35,0.49), respectively. The corresponding ML photos of $CaLaAl_3O_7$:Tb^{3+} and ZnS:Cu are presented in Fig. 7b. The above results suggest that $CaLaAl_3O_7$:Tb^{3+} is a very efficient green ML material, showing promising applications in the new generation of lighting, displaying and sensing devices.

4. Conclusions

In summary, $CaLaAl_3O_7$:Tb^{3+} powders with a layered structure were successfully synthesized by the solid-state method. When mechanics was applied, the $CaLaAl_3O_7$:Tb^{3+} could exhibit characteristic emissions of Tb^{3+} with a green color. The optimum doping concentration of Tb^{3+} for the ML of $CaLaAl_3O_7$:Tb^{3+} was determined to be 6.0%, whatever the sample was stimulated by rubbing or stretching. Temperature-dependent TL and ML properties of $CaLaAl_3O_7$:Tb^{3+} further suggest that its ML should directly originate from the de-trapped carriers under mechanics stimulation, and herein the underlying ML mechanisms were revealed. The as-obtained $CaLaAl_3O_7$:Tb^{3+} presents an extremely high ML intensity, showing promising applications in the new generation of lighting, displaying and sensing devices.

CRediT authorship contribution statement

Shiye Qin: Methodology, Validation, Investigation, Visualization, Writing – original draft. **Jiali Bian:** Validation, Investigation. **Yue Han:** Validation, Investigation. **Zhidong Ma:** Validation, Investigation. **Bin Liu:** Validation, Funding acquisition. **Jiachi Zhang:** Conceptualization, Writing – review & editing, Funding acquisition. **Xuhui Xu:** Writing – review & editing. **Zhaofeng Wang:** Conceptualization, Writing – review & editing, Funding acquisition.

Declaration of Competing Interest

The authors declare that they have no known competing financial interests or personal relationships that could have appeared to influence the work reported in this paper.

Acknowledgements

This work was supported by the National Natural Science Foundation of China (12074159 and 81970976), and the Natural Science Foundation for Distinguished Young Scholars of Gansu Province (20JR5RA572).

References

[1] Y. Xie, Z. Li, Chem. 4 (2018) 943–971.
[2] J.-C.G. Bünzli, K.-L. Wong, J. Rare. Earths 36 (2018) 1–41.
[3] J.-C. Zhang, X. Wang, G. Marriott, C.-N. Xu, Prog. Mater. Sci. 103 (2019) 678–742.
[4] Y. Zhuang, R.J. Xie, Adv. Mater. (2021), e2005925.
[5] S.M. Jeong, S. Song, K.-I. Joo, J. Kim, S.-H. Hwang, J. Jeong, H. Kim, Energy. Environ. Sci. 7 (2014) 3338–3346.
[6] Y. Zhao, D. Peng, G. Bai, Y. Huang, S. Xu, J. Hao, Adv. Funct. Mater. 31 (2021), 2010265.
[7] C. Wu, S. Zeng, Z. Wang, F. Wang, H. Zhou, J. Zhang, Z. Ci, L. Sun, Adv. Funct. Mater. 28 (2018), 1803168.
[8] X. Wang, H. Zhang, R. Yu, L. Dong, D. Peng, A. Zhang, Y. Zhang, H. Liu, C. Pan, Z. L. Wang, Adv. Mater. 27 (2015) 2324–2331.
[9] C. Chen, Y. Zhuang, X. Li, F. Lin, D. Peng, D. Tu, A. Xie, R.J. Xie, Adv. Funct. Mater. 31 (2021), 2101567.
[10] Y.-T. Fan, Y.-L. Yang, T. Li, J.-Y. Yuan, Q.-L. Li, J.-T. Zhao, D.-Y. Wan, Z.-J. Zhang, J. Mater. Chem. C. 9 (2021) 5868–5875.
[11] S.Moon Jeong, S. Song, S.-K. Lee, B. Choi, Appl. Phys. Lett. 102 (2013), 051110.
[12] Y. Du, Y. Jiang, T. Sun, J. Zhao, B. Huang, D. Peng, F. Wang, Adv. Mater. 31 (2019), e1807062.
[13] P. Jha, B.P. Chandra, J. Lumin. 143 (2013) 280–287.
[14] Y.-F. Xu, D.-K. Ma, M.-L. Guan, X.-A. Chen, Q.-Q. Pan, S.-M. Huang, J. Alloys. Compd. 502 (2010) 38–42.
[15] B. Tian, Z. Wang, A.T. Smith, Y. Bai, J. Li, N. Zhang, Z. Xue, L. Sun, Nano Energy 83 (2021), 105860.
[16] Y. Zhang, X. Yin, H. Yu, H. Cong, H. Zhang, J. Wang, R.I. Boughton, Cryst. Growth. Des. 12 (2011) 622–628.
[17] Y. Li, I.P. Koskin, Z. Ma, E. Benassi, Z. Wang, Dalton. Trans. 49 (2020) 3942–3945.
[18] H. Zhang, C.-N. Xu, N. Terasaki, H. Yamada, ECS. Solid. State. Lett. 14 (2011) J76–J80.
[19] N. Zhang, B. Tian, Z. Wang, A.T. Smith, Z. Ma, Z. Xue, L. Sun, Adv. Opt. Mater. 9 (2021), 2100137.
[20] B. Li, X. Huang, H. Guo, Y. Zeng, Dyes. Pigm. 150 (2018) 67–72.
[21] S. Sun, L. Wu, H. Yi, L. Wu, J. Ji, C. Zhang, Y. Zhang, Y. Kong, J. Xu, Opt. Express. 6 (2016) 1172–1185.
[22] V. Singh, K.N. Shinde, M.S. Pathak, N. Singh, V. Dubey, P.K. Singh, H.D. Jirimali, Optik 164 (2018) 407–413.
[23] A.P. Tsai, J. Non. Cryst. Solids 334–335 (2004) 317–322.
[24] S. Kadyan, K. Singh, S. Singh, S. Sheoran, J. Singh, D. Singh, Luminescence. 35 (2020) 673–683.
[25] K. Rawat, A.K. Vishwakarma, K. Jha, Mater. Res. Bull. 124 (2020), 110750.
[26] M. Yang, H. You, Y. Song, Y. Huang, G. Jia, K. Liu, Y. Zheng, L. Zhang, H. Zhang, J. Phys. Chem. C. 113 (2009) 20173–20177.
[27] M.H. Im, Y.J. Kim, Mater. Res. Bull. 112 (2019) 399–405.
[28] X. Guo, J. He, M. Huang, R. Shi, Y. Chen, Y. Huang, J. Zhang, Z.-Q. Liu, Mater. Res. Bull. 118 (2019), 110523.
[29] M. Shi, D. Zhang, C. Chang, J. Alloys. Compd. 627 (2015) 25–30.
[30] G. Zhang, Y. Sun, B. Qian, H. Gao, D. Zuo, Polym. Test. 90 (2020), 106670.
[31] Y. Zou, X. Min, Z. Liu, L. Yu, B. Liu, Mater. Res. Bull. 124 (2020), 110769.

[32] W. Peng, H. Xia, Z. Zhang, T. Qi, S. Kong, W. Dai, Z. Huang, J. Alloys. Compd. 753 (2018) 35–40.
[33] K. Van den Eeckhout, A.J.J. Bos, D. Poelman, P.F. Smet, Phy. Rev. B. 87 (2013), 045126.
[34] O.Q. De Clercq, J. Du, P.F. Smet, J.J. Joos, D. Poelman, Phys. Chem. Chem. Phys. 20 (2018) 30455–30465.